Bayes-optimal solution to inverse halftoning based on statistical mechanics of the Q-Ising model

(Article Cathegory: Research Article)

Yohei Saika[1], Jun-ichi Inoue [2], Hiroyuki Tanaka [3], Masato Okada [3]

[1] Department of Electrical and Computer Engineering,
Wakayama National College of Technology,
77 Noshima, Nada, Gobo, Wakayama 644-0023, Japan
email: saika@wakayama-nct.ac.jp

[2] Complex Systems Engineering,
Graduate School of Information Science and Technology,
Hokkaido University,
N14-W9, Kita-ku, Sapporo 060-0814, Japan

[3] Division of Transdisciplinary Science,
Graduate School of Frontier Science, The University of Tokyo,
5-1-5 Kashiwanoha, Kashiwa-shi, Chiba 277-8561, Japan

March 6, 2009

Abstract

On the basis of statistical mechanics of the Q-Ising model, we formulate the Bayesian inference to the problem of inverse halftoning, which is the inverse process of representing gray-scales in images by means of black and white dots. Using Monte Carlo simulations, we investigate statistical properties of the inverse process, especially, we reveal the condition of the Bayes-optimal solution for which the mean-square error takes its minimum. The numerical result is qualitatively confirmed by analysis of the infinite-range model. As demonstrations of our approach, we apply the method to retrieve a grayscale image, such as standard image *Lena*, from the halftoned version. We find that the Bayes-optimal solution gives a fine restored grayscale image which is very close to the original. In addition, based on statistical mechanics of the Q-Ising model, we are sucessful in constructing a practically useful method of inverse halftoning using the Bethe approximation.

Keywords; statistical mechanics, inverse halftoning, Monte Carlo simulation, infinite-range model, Bethe approximation
PACS; 01.30.-y, 01.30.Xx, 01.30.Tt

1 Introduction

For many years, a lot of researchers have investigated various problems in information sciences, such as image analysis based on the Markov random fields [1, 2, 3]. In recent two or three decades, a considerable number of theoretical physicists [4, 5, 6] have studied various problems, such as image restoration and error-correcting codes, based on the analogy between statistical mechanics and information processing. For instance, the mean-field theory established in statistical mechanics have been applied to image restoration [7, 8] to approximate the optimal solution. Then, Pryce and Bruce [9] have proposed the threshold posterior marginal (TPM) estimate for image restoration based on statistical mechanics of the Q-Ising model. In recent years, Nishimori and Wong [10] have constructed an unified framework based on statistical mechanics of the Ising spin glass model for the problems of image restoration and error-correcting codes. They evaluated the statistical performance via the Monte Carlo simulation and the replica theory established in the theory of spin glasses. Since their study, statistical mechanical techniques have been applied to various problems in image processing, such as the segmentation [11]. From these facts, we find that the research field, the so-called *Statistical Mechanics of Information* is now an established important subject in statistical mechanics.

In the field of the print technologies, many techniques of information processing have also developed. Particularly, the *digital halftoning* [12, 13, 14, 15, 16] is regarded as a key information processing to convert a digital grayscale image to black and white dots which represents the original grayscale levels appropriately. On the other hand, the inverse process of the digital halftoning is referred to as *inverse halftoning*. The inverse halftoning is also important for us to make scanner machines to retrieve the original grayscale image by making use of much less informative materials, such as the halftoned binary dots. The inverse halftoning is 'ill-posed' in the sense that one lacks information to retrieve the original image because the material one can utilize is just only the halftoned black and white binary dots instead of the grayscale one. To overcome this difficulty, the Bayesian approach becomes a powerful tool which is clarified to have close relation to statistical mechanics. Under the direction of this approach, Stevenson [17] attempted to apply the maximum of a Posteriori (MAP for short) estimation to the problem of inverse halftoning for a given halftone binary dots obtained by the threshold mask and the so-called error diffusion methods. However, from the theoretical point of view, there are few theoretical papers to deal with the inverse-halftoning based on the Bayesian inference and statistical mechanics of information. Besides the Bayesian approach, we usually introduce the 'regularization term' which compensates the lack of the information and regard the inverse problem as a combinatorial optimization [18, 19]. For this problem, the optimization is then achieved to find the lowest energy state via, for example, simulated annealing [20, 21].

In this study, based on the framework of statistical mechanics of the Q-Ising model [22] which is regarded as the Bayesian inference, we formulate the problem of inverse halftoning to estimate the original grayscale levels by using the information both on the halftoned binary dots and the threshold mask. Here, we reconstruct the original grayscale revels from a given halftoned binary image and the threshold mask so as to maximize the posterior marginal probability. Then, using the Monte Carlo simulation for a set of the snapshots generated with the Gibbs distribution of the Q-Ising model, we investigate statistical properties of the inverse process, especially, we reveal the condition of the Bayes-optimal solution for which the mean-square error takes its minimum. We clarify that the optimal performance is achieved around the Bayes-optimal condition that the model prior is assumed to be completely same as the true prior. Then, from the statistical

mechanical point of view, we show that the present method is carried out by constructing the equilibrium state of the Q-Ising model under the constraints coming from the halftone process, and further that the optimal performance is realized, if we appropriately set the hyperparamter corresponding to the absolute temperature. In addition, we show that the performance under the Bayes-optimal condition is superior to that of the MAP estimate, if the thresholds are not set appropriately in the halftone process. Then, in order to investigate to what extent the Bayesian approach is effective for realistic images, we apply the method to retrieve the grayscale levels of the 256-levels standard image *Lena* from the binary dots. We find that the Bayes-optimal solution gives a fine restored grayscale image which is very close to the original one. Next, from the theoretical point of view, we clarify without the statistical uncertainty that the analytical estimate of the infinite-range model supports the result of the Monte Carlo simulation for the set of the snapshots of the Q-Ising model, although the infinite-range interactions are introduced into the present model to realize the analyitical estimate. Moreover, we here construct a practically useful technique based on the Bayes inference using the Bethe approximation for inverse halftoning. Here the Bethe approximation is established in statistical mechanics to clarify thermodynamic properties of magnetic spin systems approximately. Then, the Bayes inference using the Bethe approximation is clarified to be regarded as the Belief propagation method in the field of information sciences. In this study, we indicate that the present method is effectively works for the set of the snapshots of the Q-Ising model by solving the self-consistent equations of the Bethe approximation.

The contents of this paper are organized as follows. In the next section, we formulate the problem of inverse halftoning based on statistical mechanics of the Q-Ising model. Here we mention the relationship between statistical mechanics of the Q-Ising model and Bayesian inference of the inverse halftoning. In the following section, we investigate statistical properties of the statistical mechanical inverse halftoning by Monte Carlo simulations. We also show that the Bayes-optimal inverse halftoning is useful even for realistic images, such as the 256-level standard image *Lena*. Then, analysis of the infinite-range model supports the result of the Monte Carlo simulations. We also indicate the validity of the Bethe approximation for inverse halftoning. Last section is devoted to summary.

2 The model

In this section, based on statistical mechanics of the Q-Ising model on the square lattice, we construct a Bayesian inference for the problem of inverse halftoning.

First, we consider an original grayscale image which is expressed as a snapshot from a Gibbs distribution of the ferromagnetic Q-Ising model having the spin variables $\{\xi\} \equiv \{\xi_{x,y} = 0, \cdots, Q-1 | x, y = 0, \cdots, L-1\}$. Then, each image $\{\xi\}$ follows the Gibbs distribution

$$\Pr\left(\{\xi\}\right) = \frac{1}{Z_s} \exp\left[-\frac{J_s}{T_s} \sum_{\text{n.n.}} \left(\xi_{x,y} - \xi_{x',y'}\right)^2\right] \tag{1}$$

at temperature T_s. Here Z_s which is called as the partition function in statisitcal mechanics is the normalization factor of the Gibbs distribution, namely,

$$Z_s = \prod_{x=0}^{L-1} \prod_{y=0}^{L-1} \sum_{z_{x,y}=0}^{Q-1} \exp\left[-\frac{J_s}{T_s} \sum_{\text{n.n.}} \left(\xi_{x,y} - \xi_{x',y'}\right)^2\right]. \tag{2}$$

Then, the summation $\sum_{\text{n.n.}}(\cdots)$ runs over the sets of the nearest neighboring pixels located on the square lattice in two dimension. The ratio of strength of spin-pair interaction J_s and temperature T_s, namely, J_s/T_s controls the smoothness of our original image $\{\xi\}$. In Fig. 1 (left), we show a typical example of the snapshots from the distribution (1) for the case of $Q = 4$, $J_s = 1$ and $T_s = 1$. The right panel of the Fig. 1 shows the 256-levels grayscale standard image

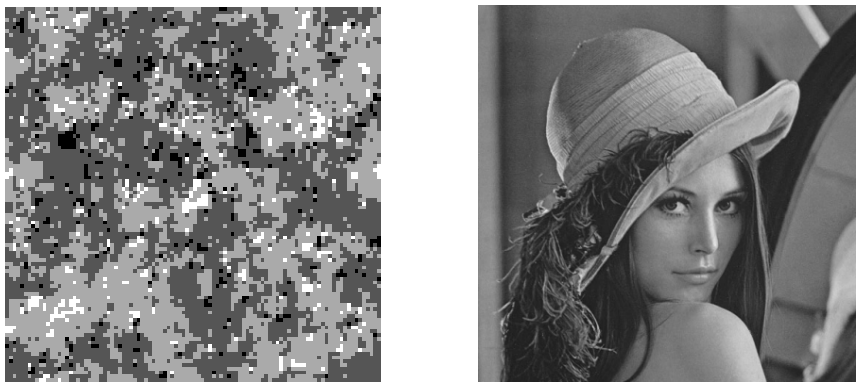

Figure 1: An original image as a snapshot from the Gibbs distribution of (1) having 100×100 pixels for the case of $Q = 4$ (left), where we set to $T_s = 1$, $J = 1$. The right panel shows a 256-levels standard image *Lena* with 400×400 pixels.

Lena with 400×400 pixels. We shall use the standard image to check the efficiency of our approach. In order to convert the original grayscale images to the the black and white binary dots, we make use of the threshold array $\{M\}$. Each component $M_{k,l}$ of the array $\{M\}$ takes

0	2
3	1

0	8	2	10
12	4	14	6
3	11	1	9
15	7	13	5

Figure 2: The Bayer-type threshold arrays for the dither method with 2×2 (left) and with 4×4 (right).

a integer from 0 to $L_m \times L_m - 1$ and these numbers are arranged on the $L_m \times L_m$ squares as shown in Fig. 2 for $L_m = 2$ (left) and for $L_m = 4$ (right). For general case of L_m, we define the array as

$$\{M\} \quad = \quad \left\{ M_{k,l} = 0, \frac{Q-1}{L_m^2 - 1}, \frac{2(Q-1)}{L_m^2 - 1}, \cdots, Q-1 \middle| k, l = 0, 1, \cdots, L_m - 1 \right\}. \tag{3}$$

We should keep in mind that the definition (3) is reduced to $\{M\} = \{M_{k,l} = 0, 1, \cdots, Q-1 | k, l = 0, 1, \cdots, \sqrt{Q}-1\}$ and the domain of each component of the threshold array becomes the same as that of the original image $\{\xi\}$ for $L_m^2 = Q$. In the dither method, we first make a pixel-to-pixel map between each element of the threshold array $M_{k,l}$ and the original grayscale $\xi_{x,y}$ at the (x, y)-th pixel considering the relations $x = pL_m + k$ and $y = qL_m + l$. Here p and q are the integers from 0 to $L/L_m - 1$. As shown in Fig. 3, we can see that this map is achieved by

arranging $(L/L_m)^2$ threshold arrays on the original grayscale image $\{\xi\}$. Next, we convert each original pixel $\xi_{x,y}$ into the binary dot $\tau_{x,y}$ by

$$\tau_{x,y} = \theta\left(\xi_{x,y} - M_{x,y}\right). \tag{4}$$

Here $M_{x,y}$ which denotes the threshold corresponding to the (x,y)-th pixel of the original image $\{\xi\}$. Then, $\theta(\cdots)$ denotes the unit-step function. Halftone images generated by the dither method via (4) are shown in Fig. 4. We find that the left panel obtained by the uniform threshold mask $M_{x,y} = 1.5\ (\forall_{x,y})$ is hard to be recognized as an original grayscale image, whereas, the center panel obtained by the 2×2 Bayer-type threshold array might be recognized as just like an original image through our human vision systems (due to a kind of *optical illusion*). Obviously, the inverse process of the above halftoning is regarded as an ill-posed problem. This is because from (4), one can not determine the original image $\xi_{x,y}\,(\forall_{x,y})$ completely from a given set of $\tau_{x,y}\,(\forall_{x,y})$ and $M_{x,y}\,(\forall_{x,y})$.

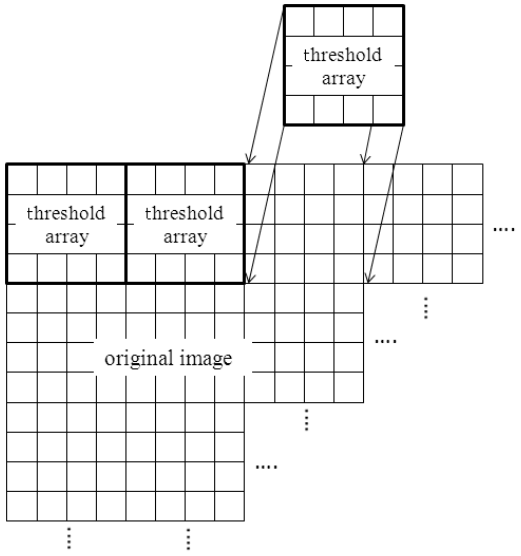

Figure 3: The pixel-to-pixel map between each element of the threshold array and the corresponding original grayscale pixel.

In this manuscript, in the procedure of the Bayesian inverse digital halftoning, we attempt to restore the original grayscale image from a given halftone image by means of the so-called maximizer of posterior marginal (MPM for short) estimate. In this method, we define $\{z\} = \{z_{x,y} = 0, \cdots, Q-1 | x, y = 0, \cdots, L-1\}$ as an estimate of the original image $\{\xi\}$ which is arranged on the square lattice and reconstruct the grayscale image on the basis of maximizing the following posterior marginal probability:

$$\hat{z}_{x,y} \;=\; \arg\max_{z_{x,y}} \sum_{\{z\}\neq z_{x,y}} \Pr(\{z\}|\{\tau\}) = \arg\max_{z_{x,y}} \Pr\left(z_{x,y}|\{\tau\}\right), \tag{5}$$

where the summation $\sum_{z_{x,y}\neq\{z\}}(\cdots)$ runs over all pixels except for the (x,y)-th pixel and the posterior probability $P(\{z\}|\{\tau\})$ is estimated by the Bayes formula:

$$\Pr\left(\{z\}|\{\tau\}\right) = \frac{\Pr\left(\{z\}\right)\Pr\left(\{\tau\}|\{z\}\right)}{\sum_{\{z\}}\Pr\left(\{z\}\right)\Pr\left(\{\tau\}|\{z\}\right)} \tag{6}$$

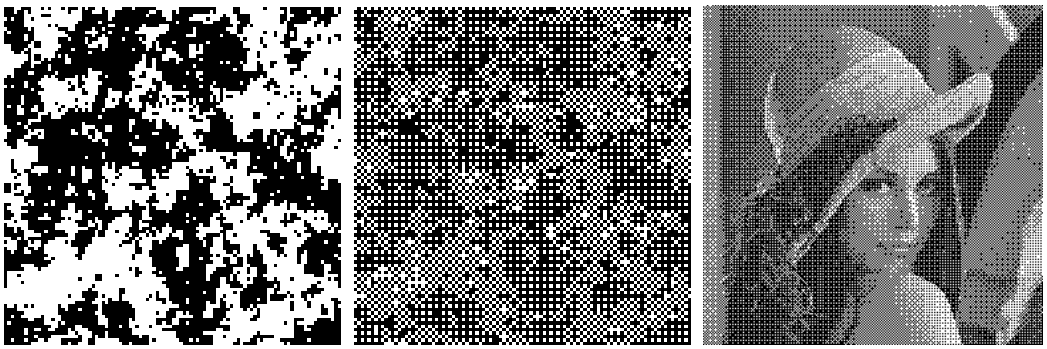

Figure 4: The left panel shows a halftone image converted by the dither method using the uniform threshold $M = 2$ from the snapshot from a Gibbs distribution of the $Q = 4$ Ising model shown in Fig. 1 (left). The center panel shows a halftone image obtained by the dither method using the 2×2 Bayer-type threshold array from the same snapshot. The right panel shows a halftone image converted by the dither method using the 4×4 Bayer-type threshold array from the 256-level standard image *Lena* with 400×400 pixels shown in Fig. 1 (right).

In this study, following Stevenson [17], we assume that the likelihood might have the same form as the halftone process of the dither method, namely,

$$P\left(\{\tau\}|\{z\}\right) = \Pi_{(x,y)}\delta\left(\tau_{x,y}, \theta\left(z_{x,y} - M_{x,y}\right)\right), \tag{7}$$

where $\delta(a, b)$ denotes a Kronecker delta and we should notice that the information on the threshold array $\{M\}$ is available in addition to the halftone image $\{\tau\}$. Then, we choose the model of the true prior as

$$\Pr(\{z\}) = \frac{1}{Z_m} \exp\left[-\frac{J}{T_m} \sum_{\text{n.n.}} \left(z_{x,y} - z_{x',y'}\right)^2\right], \tag{8}$$

where Z_{m} is a normalization factor. J and T are the so-called hyper-parameters. It should be noted that one can construct the Bayes-optimal solution if we assume that the model prior has the same form as the true prior, namely, $J = J_s$ and $T_m = T_s$ (what we call, *Nishimori line* in the research field of spin glasses [4]).
From the viewpoint of statistical mechanics, the posterior probability $\Pr(\{z\}|\{\tau\})$ generates the equilibrium states of the ferromagnetic Q-Ising model whose Hamiltonian is given by

$$H\left(\{z\}\right) = J \sum_{\text{n.n.}} \left(z_{x,y} - z_{x',y'}\right)^2, \tag{9}$$

under the constraints

$$\forall_{x,y} \quad \tau_{x,y} - \theta\left(z_{x,y} - M_{x,y}\right) = 0. \tag{10}$$

Obviously, the number of possible spin configurations that satisfy the above constraints (10) is evaluated as $\prod_{(x,y)} |Q\tau_{x,y} - M_{x,y}|$ and this quantity is exponential order such as $\sim \alpha^{L^2}$ (α: a positive constant). Therefore, the solution $\{z\}$ to satisfy the constraints (10) is not unique and this fact makes the problem very hard. To reduce the difficulties, we consider the equilibrium state generated by a Gibbs distribution of the ferromagnetic Q-Ising model with the constraints (10) and increase the parameter J gradually from $J = 0$. Then, we naturally expect that the system stabilizes the ferromagnetic Q-Ising configurations due to a kind of the regularization

term (9). Thus, we might choose the best possible solution among a lot of candidates satisfying (10).
From the view point of statistical mechanics, the MPM estimate is rewritten by

$$\hat{z}_{x,y} = \Theta_Q(\langle z_{x,y}\rangle), \quad \langle z_{x,y}\rangle = \sum_z z_{x,y}\Pr(\{z\}|\{\tau\}) \tag{11}$$

where $\Theta_Q(\cdots)$ is the Q-generalized step function defined by

$$\theta_Q(x) = \sum_{k=0}^{Q-1} k\left\{\theta\left(x-\left(k-\frac{1}{2}\right)\right)-\theta\left(x-\left(k+\frac{1}{2}\right)\right)\right\}. \tag{12}$$

Obviously, $\langle z_{x,y}\rangle$ is a local magnetization of the system described by (9) under (10).

2.1 Average case performance measure

To investigate the performance of the inverse halftoning, we evaluate the mean square error which represents the pixel-wise similarity between the original and restored images. Especially, we evaluate the average case performance of the inverse halftoning through the following averaged mean square error

$$\sigma = \frac{1}{Q^2L^2}\sum_{\{\xi\}}\Pr\left(\{\xi\}\right)\sum_{(x,y)}\left(\hat{z}_{x.y}-\xi_{x,y}\right)^2. \tag{13}$$

We should keep in mind that the σ gives zero if all restored images are exactly the same as the corresponding original images.

3 Results

In this section, we first investigate the statistical properties of our approach to the inverse halftoning for a set of snapshots from a Gibbs distribution of the ferromagnetic Q-Ising model via computer simulations. Then, we check the usefulness of our approach for the realistic images, namely, the 256-levels standard image *Lena*. We next analytically evaluate the performance for the infinite-range model. Moreover, in order to construct a practically useful method, we propose a Bayesian inference using the Bethe approximation.

3.1 Monte Carlo simulation

We first carry out Monte Carlo simulations for a set of halftone images, which are obtained from the snapshots of the $Q = 4$ Ising model with 100×100 pixels by the dither method using the uniform thresholds $M_{x,y} = 3/2$ $(\forall_{x,y})$, $M_{x,y} = 1/2$ $(\forall_{x,y})$ and the 2×2 Bayer-type threshold array as shown in Fig. 2. In order to clarify the statistical performance of our method, we reveal the hyper-parameters J and T_m dependence of the averaged mean square error σ. For this purpose, we use 10 snapshots of the ferromagnetic $Q = 4$ Ising model $\{\xi_{x,y}\}$ with 100×100 pixels on the square lattice. These images are generated by the Monte Carlo simulation based on the Metropolis algorithm with 20000 Monte Carlo steps (MCS, for short) from a random pattern at $T_{\rm s} = 1$. Then, when we restore the grayscale image, we carry out the Monte Carlo simulation based on the Metropolis algorithm with 20000 MCS at assumed temperature $T_{\rm m}$,

starting from the halftone image $\{\tau\}$. Here the halftone image $\{\tau\}$ is obviously satisfied with the constraint $\delta(\theta(\xi_{x,y}-M_{x,y}),\theta(z_{x,y}-M_{x,y}))=1$ at each pixel. As shown in Fig. 5 (a), we first investigate the hyperparameter $T_{\rm m}$ dependence of the mean square error when the threshold are set to $M=3/2$ under the conditions, $Q=4$, $T_{\rm s}=1$, $J_{\rm s}=1$, $J=1$. This figure shows that the present method achieves the best possible performance under the Bayes-optimal condition, that is, $J=J_s$ and $T_m=T_s$, and that the limit $T_m\to\infty$ leading up to the MAP estimate gives almost the same performance as the Bayes-optimal MPM estimate. This fact means that it is not necessary for us to take the $T_{\rm m}\to 0$ limit when we carry out the inverse halftoning via simulated annealing. On the other hand, as shown in Fig. 5 (b), we show the $T_{\rm m}$ dependence of the mean square error for the case that the threshold is set to $M_{x,y}=1/2$ at each pixel. Here we set other parameters as $Q=4$, $T_{\rm s}=1$, $J_{\rm s}=1$ and $J=1$. In this case, as is same as the $M_{x,y}=3/2$, we also confirm that the optimal performance is achieved under the Bayes-optimal condition. However, this figure indicates that the performance under the Bayes-optimal condition is superior to that of the $T_{\rm m}\to 0$ limit of the present method. From the statistical mechanical point of view, this result suggests that the thermal fluctuations enable us to improve the performance of the present method by tuning the absolute temperature $T_{\rm m}$ to the Bayes-optimal condition. These results indicate that the performance of the present method under the Bayes-optimal condition is at least superior to the MAP estimate. From the restored image in Fig. 6 (center), it is actually confirmed that the present method effectively works for the snapshot of the ferromagnetic Q-Ising model. It should be noted that the mean square error evaluated for the 2×2 Bayer-type array is larger than that for the $M=2$ uniform threshold. This result seems to be somewhat counter-intuitive because the halftone image shown in the center panel of Fig. 4 seems to be much closer to the original image, in other words, is much informative to retrieve the original image than the halftone image shown in the left panel of the same figure. However, it could be understood as follows. The shape of each 'cluster' appearing in the original image (see the left panel of Fig. 1) remains in the halftone version (the left panel of Fig. 4), whereas, in the halftone image (the center panel of Fig. 4), such structure is destroyed by the halftoning process via the 2×2 Bayer-type array. As we found, in a snapshot of the ferromagnetic Q-Ising model at the inverse temperature $J_s/T_s=1$, the large size clusters are much more dominant components than the small isolated pixels. Therefore, the averaged mean square error is sensitive to the change of the cluster size or the shape, and if we use the constant threshold mask to create the halftone image, the shape of the cluster does not change, whereas the high-frequency components vanish. These properties are desirable for us to suppress the increase of the averaged mean square error. This fact implies us that the averaged mean square error for the 2×2 Bayer-type is larger than that for the constant mask array and the performance is much worse than expected.

Moreover, the above evaluations might be helpful for us to deal with the inverse halftoning from the halftoned image of the standard image with confidence. In fact, we are also confirmed that our method is practically useful from the resulting image shown in Fig. 6 (right) having the mean square error $\sigma=0.002005$.

3.2 Analysis of the infinite-range model

In this subsection, we check the validity of our Monte Carlo simulations, namely, we analytically evaluate the statistical performance of the present method for a given set of the snapshots from a Gibbs distribution of the ferromagnetic Q-Ising model in which each spin variable is located on the vertices of the complete graph. For simplicity, we first transform the index from (x,y)

to i so as to satisfy $i = x + Ly + 1$. Then, the new index i runs from $i = 1$ to $L^2 - 1 = N$. For this new index of each spin variable, we consider the infinite-range version of true prior and the model as

$$\Pr(\{\xi\}) = \frac{\mathrm{e}^{-\frac{\beta_{\mathrm{s}}}{2N}\sum_{i<j}(\xi_i-\xi_j)^2}}{Z_{\mathrm{s}}},\ \Pr(\{z\}) = \frac{\mathrm{e}^{-\frac{\beta_{\mathrm{m}}}{2N}\sum_{i<j}(z_i-z_j)^2}}{Z_{\mathrm{m}}} \tag{14}$$

where the scaling factors $1/N$ appearing in front of the sums $\sum_{i<j}(\cdots)$ are needed to take a proper thermodynamic limit. We also set $\beta_{\mathrm{s}} \equiv J_{\mathrm{s}}/T_{\mathrm{s}}$ and $\beta_{\mathrm{m}} \equiv J/T_{\mathrm{m}}$ for simplicity. Obviously, Z_{s} and Z_{m} in (13) are the normalization factors of the infinite-range versions of model and true priors.

In order to investigate the statistical performance of present method, we here estimate the thermodynamic properties of the system $\{z\}$ in terms of the free energy as

$$\begin{aligned}[\langle f\rangle]_{\xi} = -\beta_{\mathrm{m}}^{-1}\sum_{\{\xi\}}\frac{\mathrm{e}^{-\frac{\beta_{\mathrm{s}}}{2N}\sum_{i<j}(\xi_i-\xi_j)^2}}{Z_{\mathrm{s}}} \\ \times\log\left[\sum_{\{z\}}\mathrm{e}^{-\frac{\beta_{\mathrm{m}}}{2N}\sum_{i<j}(z_i-z_j)^2}\Pi_i\delta\left(\theta(\xi_i-M_i),\theta(z_i-M_i)\right)\right],\end{aligned} \tag{15}$$

Here $[\langle\cdots\rangle]_{\xi}$ means thermal average of some physical quantities $(\cdots)$ averaged over the infinite-range version of the true prior $P(\{\xi\})$ as quenched disorders. The thermodynamic properties of the system $\{z\}$ are clarified from the saddle-point conditions of the free energy both on the magnetization m_0 of the original image $\{\xi\}$ and the magnetization m for the restored pixels $\{z\}$ as

$$\frac{\partial[\langle f\rangle]_{\xi}}{\partial m_0} = 0,\ \ \frac{\partial[\langle f\rangle]_{\xi}}{\partial m} = 0. \tag{16}$$

Throughout the straightforward calculation, we can derive the explicit forms of the self-consistent equations of m_0 and m as

$$m_0 \equiv \frac{1}{N}\sum_{i=1}^{N}\xi_i = \frac{\sum_{\xi=0}^{Q-1}\xi\exp[2\beta_s m_0\xi - \beta_s\xi^2]}{\sum_{\xi=0}^{Q-1}\exp[2\beta_s m_0\xi - \beta_s\xi^2]}. \tag{17}$$

$$m \equiv \frac{1}{N}\sum_{i=1}^{N}z_i = \frac{\sum_{\xi=0}^{Q-1}\left(\frac{\sum_{z=0}^{Q-1}z\,\mathrm{e}^{2\beta_m mz-\beta_m z^2}\delta(\theta(\xi-M),\theta(z-M))}{\sum_{z=0}^{Q-1}\mathrm{e}^{2\beta_m mz-\beta_m z^2}\delta(\theta(\xi-M),\theta(z-M))}\right)\mathrm{e}^{2\beta_s m_0\xi-\beta_s\xi^2}}{\sum_{\xi=0}^{Q-1}\mathrm{e}^{2\beta_s m_0\xi-\beta_s\xi^2}}. \tag{18}$$

Then, the average case performance is determined by the following averaged mean square error:

$$\begin{aligned}\sigma &\equiv \frac{1}{NQ^2}\sum_{i=1}^{N}\{\xi_i - \Theta_Q(\langle z_i\rangle)\}^2 \\ &= \frac{\sum_{\xi=0}^{Q-1}\left\{\xi - \Theta_Q\left(\frac{\sum_{z=0}^{Q-1}z\,\mathrm{e}^{2\beta_m mz-\beta_m z^2}\delta(\theta(\xi-M),\theta(z-M))}{\sum_{z=0}^{Q-1}\mathrm{e}^{2\beta_m mz-\beta_m z^2}\delta(\theta(\xi-M),\theta(z-M))}\right)\right\}^2\mathrm{e}^{2\beta_s m_0\xi-\beta_s\xi^2}}{Q^2\sum_{\xi=0}^{Q-1}\mathrm{e}^{2\beta_s m_0\xi-\beta_s\xi^2}}\end{aligned} \tag{19}$$

Solving these self-consistent equations with respect to m_0 in Eq. (17) and m in Eq. (18), we evaluate the statistical performance of the present method through the quantity σ (19) analytically.
As we have mentioned using the Monte Carlo simulation, we estimate how the mean square error depends on the hyper-parameter T_m for the infinite-range version of our model when we set to $Q = 8$, $J_s = 1$, $T_s = 1$, $M = 3.5\,(= (Q-1)/2), 4.5$ and $J = 1$. We find from Figs. 7 (a) and (b) that the mean square error takes its minimum in the wide range on T_m including the Bayes-optimal condition $T_m = T_s\,(= 1)$. Here, we note that $m = m_0\,(= 3.5)$ holds under the Bayes-optimal condition, $T_m = T_s$ for both cases of $M = 3.5$ and $M = 4.5$, which is shown in Fig. 8. From this fact, we might evaluate the gap Δ between the lowest value of the mean square error and the second lowest value obtained at the higher temperature than T_s as follows.

$$\begin{aligned}\Delta &\simeq \frac{\sum_{\xi=0}^{Q-1}(\xi - m_0)^2 \mathrm{e}^{2\beta_s m_0 \xi - \beta_s \xi^2}}{Q^2 \sum_{\xi=0}^{Q-1} \mathrm{e}^{2\beta_s m_0 \xi - \beta_s \xi^2}} - \frac{\sum_{\xi=0}^{Q-1}(\xi - m_0 - 1)^2 \mathrm{e}^{2\beta_s m_0 \xi - \beta_s \xi^2}}{Q^2 \sum_{\xi=0}^{Q-1} \mathrm{e}^{2\beta_s m_0 \xi - \beta_s \xi^2}} \\ &= \frac{\sum_{\xi=0}^{Q-1}(2\xi - 2m_0 + 1) \mathrm{e}^{2\beta_s m_0 \xi - \beta_s \xi^2}}{Q^2 \sum_{\xi=0}^{Q-1} \mathrm{e}^{2\beta_s m_0 \xi - \beta_s \xi^2}} = \frac{1}{Q^2} \end{aligned} \tag{20}$$

For example, for $Q = 8$, we evaluate the gap as $\Delta = (8)^{-2} = 0.00156$ and this value agree with the result shown in Fig. 7. From Figs. 7 and 8, we also find that the range of T_m in which the mean square error takes the lowest value coincides with the range of temperature T_m for which the magnetization satisfies $m(T_m) = m(T_s = 1) \pm 1 = 3.5 \pm 1$ as shown in Fig. 8. This robustness for the hyper-parameter selecting is one of the desirable properties from the view point of the practical use of our approach. Further, in order to clarify the validity of thermal fluctuations, we observe the gray-level distribution shown in 9. This means that thermal fluctuations due to the appropriate temperature T_m generates the appropriate gray-level distribution shown in 9(a). Then, as shown in 9 (b), if T_m is set to be smaller than the optimal value ($T_m = 0.1$), the gray-level distribution of the restored image is similar to the initial state. On the contrary, as shown in 9 (b), if T_m is set to be larger than the optimal value ($T_m = 5.0$), the gray-level distribution becomes broad due to thermal fluctuations.

3.3 Bethe approximation

In this section, we construct a practically useful method to inverse halftoning by making use of the Bethe approximation which is established in statistical mechanics to approximate the thermodynamic properties of magnetic spin systems. Then, we investigate the statistical performance of the Bethe approximation to inverse halftoning based on the mean square error.
First, we indicate how to apply the Bethe approximation to the MPM estimate. For convenience, we here note the marginal probability distributions $\Pr\left(\xi_{x,y}|\{\tau\}\right)$, $\Pr\left(\xi_{x,y}, \xi_{x',y'}|\{\tau\}\right)$ as $\rho_{x,y}\left(\xi_{x,y}\right)$, $\rho_{x,y}^{x',y'}\left(\xi_{x,y}, \xi_{x',y'}\right)$. The definition of the marginal probability distributions we use here are

$$\rho_{x,y}\left(z_{x,y}\right) = \sum_{\{\zeta\}} \delta(z_{x,y}, \zeta_{x,y}) \rho\left(\{\zeta\}\right), \tag{21}$$

$$\rho_{x,y}^{x',y'}\left(z_{x,y}, z_{x',y'}\right) = \sum_{\{\zeta\}} \delta(z_{x,y}, \zeta_{x,y}) \delta(z_{x',y'}, \zeta_{x',y'}) \rho\left(\{\zeta\}\right), \tag{22}$$

for the probability distribution:

$$\rho\left(\{z\}\right)=\frac{\prod_{(x,y)}\psi_{x,y}\left(z_{x,y}\right)\prod_{\mathrm{n.n.}}\phi_{x,y}^{x',y'}\left(z_{x,y},z_{x',y'}\right)}{\sum_{\{\zeta\}}\prod_{(x,y)}\psi_{x,y}\left(\zeta_{x,y}\right)\prod_{\mathrm{n.n.}}\phi_{x,y}^{x',y'}\left(\zeta_{x,y},\zeta_{x',y'}\right)}. \tag{23}$$

Here we set as $\psi_{x,y}(z)=\delta\left(\tau,\theta(z-M)\right)$ and $\phi_{x,y}^{x',y'}(z,z')=\exp\left[-J\left(z-z'\right)^2\right]$, where $z,z'=0,\cdots,Q-1$. In the framework of the Bethe approximation, we first consider the Bethe free energy which is given by

$$\begin{aligned}&F\left[\rho_{x,y}(z),\rho_{x,y}^{x+1,y}(z,z'),\rho_{x,y}^{x,y+1}(z,z')|x,y=0,\cdots,L-1,z,z'=0,1,\cdots,Q-1\right]\\&=E\left[\rho_{x,y}(z),\rho_{x,y}^{x+1,y}(z,z'),\rho_{x,y}^{x,y+1}(z,z')\right]-S\left[\rho_{x,y}(z),\rho_{x,y}^{x+1,y}(z,z'),\rho_{x,y}^{x,y+1}(z,z')\right].\end{aligned} \tag{24}$$

at $T_{\mathrm{m}}=1$. Here the first term in the right-hand side is the energy:

$$\begin{aligned}&E\left[\rho_{x,y}(z),\rho_{x,y}^{x+1,y}(z,z'),\rho_{x,y}^{x,y+1}(z,z')\right]\\&=-\sum_{(x,y)}\sum_{\zeta=0}^{Q-1}\Big[\log\delta\left(\tau,\theta(z-M)\right)\Big]\rho_{x,y}\left(z\right)\\&\quad+J\sum_{(x,y)}\sum_{z=0}^{Q-1}\sum_{z'=0}^{Q-1}\left(z-z'\right)\left(\rho_{x,y}^{x+1,y}\left(z,z'\right)+\rho_{x,y}^{x,y+1}\left(z,z'\right)\right).\end{aligned} \tag{25}$$

Then, the second term in the right-hand side is the entropy:

$$\begin{aligned}&S\left[\rho_{x,y}(z),\rho_{x,y}^{x+1,y}(z,z'),\rho_{x,y}^{x,y+1}(z,z')\right]\\&=S_{x,y}+\left(S_{x,y}^{x+1,y}-S_{x,y}-S_{x+1,y}\right)+\left(S_{x,y}^{x,y+1}-S_{x,y}-S_{x,y+1}\right),\end{aligned} \tag{26}$$

where

$$S_{x,y}=-\sum_{z=0}^{Q-1}\rho_{x,y}\left(z\right)\log\rho_{x,y}\left(z\right), \tag{27}$$

$$S_{x,y}^{x',y'}=-\sum_{z=0}^{Q-1}\sum_{z'=0}^{Q-1}\rho_{x,y}^{x',y'}\left(z,z'\right)\log\rho_{x,y}^{x',y'}\left(z,z'\right). \tag{28}$$

We note that $S[\rho_{x,y}(z),\rho_{x,y}^{x+1,y}(z,z'),\rho_{x,y}^{x,y+1}(z,z')]$ is an approximation of the entropy $S=-\sum_{\{z\}}\rho(\{z\})\log\rho(\{z\})$ based on the Bethe approximation. Then, we derive the deterministic equations on the set of the messages $\{\mu_{(x',y')\to(x,y)}(z)\}$ $(z=0,\cdots,Q-1)$ based on the variational principle of the Bethe free energy with respect to $\rho_{x,y}(z)$, $\rho_{x,y}^{x+1,y}(z)$ and $\rho_{x,y}^{x+1,y}(z)$ under the normalization conditions:

$$\begin{aligned}&\sum_{z=0}^{Q-1}\rho_{x,y}\left(z\right)=\sum_{z=0}^{Q-1}\sum_{z'=0}^{Q-1}\rho_{x,y}^{x+1,y}\left(z,z'\right)=\sum_{z=0}^{Q-1}\sum_{z'=0}^{Q-1}\rho_{x,y}^{x,y+1}\left(z,z'\right)\\&=\sum_{z=0}^{Q-1}\sum_{z'=0}^{Q-1}\rho_{x,y}^{x-1,y}\left(z',z\right)=\sum_{z=0}^{Q-1}\sum_{z'=0}^{Q-1}\rho_{x,y}^{x,y-1}\left(z',z\right)=1.\end{aligned} \tag{29}$$

and the reducibility conditions:

$$\rho_{x,y}(z)=\sum_{z'=0}^{Q-1}\rho_{x,y}^{x+1,y}(z,z')=\sum_{z'=0}^{Q-1}\rho_{x,y}^{x,y+1}(z,z')=\sum_{z'=0}^{Q-1}\rho_{x,y}^{x-1,y}(z',z)=\sum_{z'=0}^{Q-1}\rho_{x,y}^{x,y-1}(z',z). \tag{30}$$

using the Lagrange multipliers. Here, the set of messages $\{\mu_{(x',y')\to(x,y)}(z)\}$ is defined using the Lagrange multipliers which are introduced to ensure the normalization and reducibility conditions. As the detailed definition of the messages $\{\mu_{(x',y')\to(x,y)}(z)\}$ and the derivation of the deterministic equations on $\{\mu_{(x',y')\to(x,y)}(z)\}$ are similar to that of the conventional Bethe approximation which is shown in [5], we merely show the results of the variational calculation in the Bethe approximation. The obtained deterministic equations on the set of the messages $\{\mu_{(x',y')\to(x,y)}(z)\}$ $(z=0,\cdots,Q-1)$ are

$$\mu_{(x',y')\to(x,y)}(z)=\frac{\sum_{z'=0}^{Q-1}\phi_{x,y}^{x',y'}(z,z')\,\psi_{x',y'}(z')\prod_{(x'',y'')\in D(x',y')\backslash(x,y)}\mu_{(x'',y'')\to(x',y')}(z')}{\sum_{\zeta'=0}^{Q-1}\sum_{\zeta=0}^{Q-1}\phi_{x,y}^{x',y'}(\zeta',\zeta)\,\psi_{x',y'}(\zeta)\prod_{(x'',y'')\in D(x',y')\backslash(x,y)}\mu_{(x'',y'')\to(x',y')}(\zeta)}, \tag{31}$$

from the (x',y')-th pixel to the (x,y)-th pixel. Here $D(x,y)$ is the set of the lattice points of the nearest neighbors to the (x,y)-th pixel, namely, $\{(x+1,y),(x-1,y),(x,y+1),(x,y-1)\}$ and $D(x',y')\backslash(x,y)$ is the set of the lattice points of the nearest neighbors to the (x',y')-th pixel exept for the (x,y)-th pixel. By making use of the solution of the set of the messages $\{\hat{\mu}_{(x',y')\to(x,y)}(z)\}$, we can estimate the marginal probability distribution $\hat{\rho}_{x,y}(z)$ and the thermal average of the local magnetization $\langle z_{x,y}\rangle$ at the (x,y)-th pixel by

$$\hat{\rho}_{x,y}(z)=\frac{\psi_{x,y}(z)\prod_{(x',y')\in D(x,y)}\hat{\mu}_{(x',y')\to(x,y)}(z)}{\sum_{\zeta=0}^{Q-1}\psi_{x,y}(\zeta)\prod_{(x',y')\in D(x,y)}\hat{\mu}_{(x',y')\to(x,y)}(\zeta)}, \tag{32}$$

$$\langle z_{x,y}\rangle=\sum_{z=0}^{Q-1}z\hat{\rho}_{x,y}(z). \tag{33}$$

When we actually carry out the Bethe approximation, we derive the solution of the set of the messages $\{\mu_{(x',y')\to(x,y)}(z)\}$ using the following procedure.

Algorithm

Step 1: First set the initial condition of the set of the messages $\{\mu^{(0)}_{(x,y)\to(x',y')}(z)\}$ appropriately.

Step 2: Then, by making use of the set of the messages $\{\mu^{(k)}_{x,y\to x',y'}(z)\}$ $(k=0,1,2,\cdots)$, calculate the set of the messages $\mu^{(k+1)}_{x,y\to x',y'}(z)$ in terms of the deterministic equations:

$$\mu^{(k+1)}_{(x',y')\to(x,y)}(z)=\frac{\sum_{\zeta=0}^{Q-1}\phi_{x,y}^{x',y'}(z,\zeta)\,\psi_{x',y'}(\zeta)\prod_{(x'',y'')\in D(x',y')\backslash(x,y)}\mu^{(k)}_{(x'',y'')\to(x',y')}(\zeta)}{\sum_{\zeta'=0}^{Q-1}\sum_{\zeta=0}^{Q-1}\phi_{x,y}^{x',y'}(\zeta',\zeta)\,\psi_{x',y'}(\zeta)\prod_{(x'',y'')\in D(x',y')\backslash(x,y)}\mu^{(k)}_{(x'',y'')\to(x',y')}(\zeta)}, \tag{34}$$

where k is the number of the iteration for the deterministic equations on $\{\mu^{(k)}_{(x',y')\to(x,y)}(z)\}$.

Step 3: If

$$\frac{1}{L^2}\sum_{(x,y)}\sum_{z=0}^{Q-1}\left(\mu^{(k+1)}_{(x',y')\to(x,y)}(z)-\mu^{(k)}_{(x',y')\to(x,y)}(z)\right)^2<\epsilon \tag{35}$$

is satisfied, we regard $\{\mu^{(k+1)}_{(x',y')\to(x,y)}(z)\}$ as the solution of the equations, $\{\hat{\mu}_{(x',y')\to(x,y)}(z)\}$ and go to *Step 4*. Otherwise, go to *Step 2* and then repeat the procedure in *Step 2*. In this study, we set to $\epsilon = 1.0\times10^{-5}$.
Step 4: Calculate the pixel value of the restored grayscale image as

$$\hat{z}_{x,y}=\frac{\sum_{z=0}^{Q-1} z\ \psi_{x,y}(z)\prod_{(x',y')\in D(x,y)}\hat{\mu}_{(x',y')\to(x,y)}(z)}{\sum_{\zeta=0}^{Q-1}\psi_{x,y}(\zeta)\prod_{(x',y')\in D(x,y)}\hat{\mu}_{(x',y')\to(x,y)}(\zeta)} \tag{36}$$

by making use of the set of the solutions $\{\hat{\mu}_{(x',y')\to(x,y)}(z)\}$ for the deterministic equations.

Then, in order to clarify the efficiency of the Bethe approximation to inverse halftoning, we investigate statistical properties for the set of the snapshots of the Q-Ising model with 100×100 pixels. As shown in Figs. 10 (a) and (b), we find that the Bethe approximation accurately restores the grayscale images under the Bayes-optimal condition $T_m = T_s = 1$ and $J = J_s = 1$ and that the optimal performance of the Bethe approximation ($\hat{\sigma} = 0.004421\pm0.000075$ for $M=(Q-1)/2$ and $\hat{\sigma}=0.015123\pm0.000025$ for the 2×2 Bayer's threshold array case) is slightly inferior to that of the Monte Carlo simulatons ($\hat{\sigma}=0.004426\pm0.000157$ for $M=(Q-1)/2$ and $\hat{\sigma}=0.014861\pm0.000091$ for the 2×2 Bayer's threshold array case).

4 Summary

In this paper, we investigated the condition to achieve the Bayes-optimal performance of inverse halftoning based on statistical mechancs of the Q-Ising model by making use of computer simulations, analysis of the infinite range model and the Bethe approximation. Especially, from the statistical mechanical point of view, we clarify that the present method achieves the optimal performance for the set of the snapshots of the Q-Ising model, when we appropriately tune the hyperparameter which is regarded as the absolute temperature. We were also confirmed that our Bayesian approach is useful even for the inverse halftoning from the binary dots obtained from standard images, in the wide range on T_m including the Bayes-optimal condition, $T_m = T_s$. Moreover, we are sucessful in constructing the practically useful technique for inverse halftoning based on the MPM estimate using the Bethe approximation.
We hope that some modifications of the prior distribution might make the quality of the inverse halftoning much better. It will be our future work.

Acknowledgment

We were financially supported by *Grant-in-Aid Scientific Research on Priority Areas "Deepening and Expansion of Statistical Mechanical Informatics (DEX-SMI)" of The Ministry of Education, Culture, Sports, Science and Technology (MEXT)* No. 18079001.

References

[1] J. Besag, J. Roy. Stat. Soc. B **48**, no. 3, 259 (1986).

[2] R.C. Gonzales and R.C. Woods, *Digital Image Processing*, Addison Wesley, Reading, MA. (1992).

[3] G. Winkler, *Image Analysis, Random fields and Markov Chain Monte Carlo Methods*, Springer (2002).

[4] H. Nishimori, *Statistical Physics of Spin Glasses and Information Processing: An Introduction*, Oxford University Press, London (2001).

[5] K. Tanaka, J. Phys. A: Math. Gen. **35**, R81 (2002).

[6] N. Sourlas, Nature **339**, 693 (1989).

[7] K. Tanaka and T. Morita, Physics Letters, **203**, 122 (1995).

[8] J. Zhang, IEEE Transaction on Image Processing, **5**, 1208 (1996).

[9] J.M. Pryce and D. Bruce, J. Phys. A: Math. Gen. **28**, 511(1995).

[10] H. Nishimoi and K. Y. M. Wong, Phys. Rev. E, **6**, 132 (1999).

[11] M. Okada, K. Doya, T. Yoshioka and M. Kawato, Technical Report of IEICE, NC98-184, 239 (1999).

[12] R. Ulichney, *Digital Halftoning*, MIT Press, Massachusetts (1987).

[13] B.E. Bayer, ICC CONF. RECORD, 11 (1973).

[14] R. W. Floyd and L. Steinberg, SID Int. Sym. Digest of Tech. Papers, 36 (1975).

[15] C.M. Miceli and K.J. Parker, J. Electron Imaging **1**, 143(1992).

[16] P.W. Wong, IEEE Trans. on Image Processing **4**, 486(1995).

[17] R.L. Stevenson, IEEE **6**, 574(1997).

[18] S.D. Cabrera, K. Iyer, G. Xiang and V. Kreinovich: *On Inverse Halftoning: Computational Complexity and Interval Computations, 2000 Conference on Information Science and Systems*, The Johns Hopkins University, March 16-18 (2005).

[19] M. Discepoli and I. Greace, *Lecture Note on Computer Science* **3046**, 388 (2004).

[20] S. Kirkpatrick, C.D. Gelatt and M.P. Vecchi, Science **220**, 671 (1983).

[21] S. Geman and D. Geman, IEEE Trans. Pattern Anal. and Mach. Intel. **11**, 721 (1989).

[22] D. Bollé, H. Rieger and G.M. Shim, J. Phys. A: Math. Gen. **27**, 3411 (1994).

[23] Y. Saika and J. Inoue, in preparation.

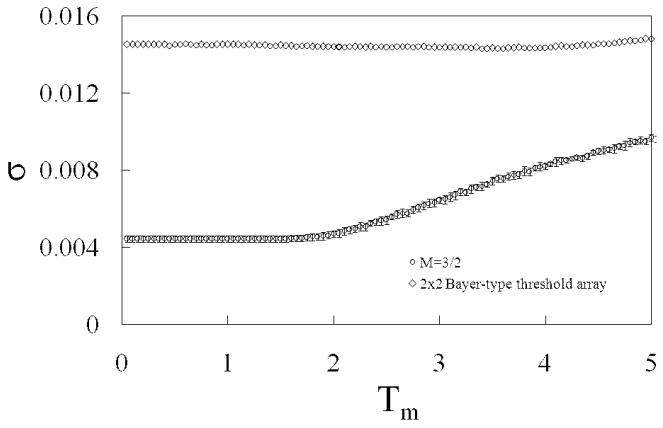

(a)

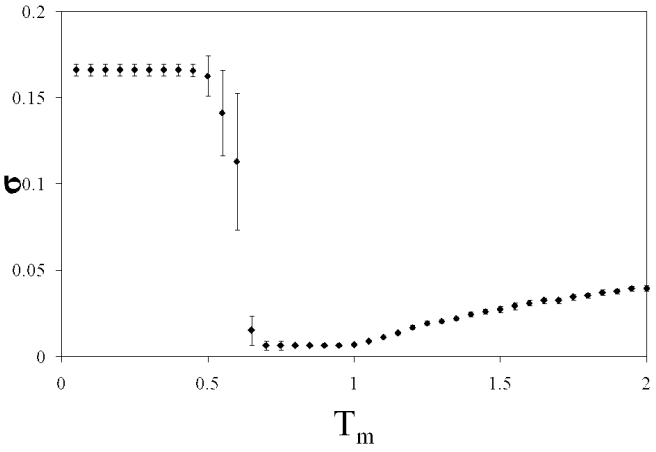

(b)

Figure 5: (a) The mean square error as a function of T_m. The original image is a snapshot from a Gibbs distribution of the $Q = 4$ ferromagnetic Ising model with 100×100 pixels and $T_s = 1.0$, $J_s = 1$ and $J = 1$. The halftone images are obtained by the uniform threshold $M = 3/2$ and 2×2 Bayer-type arrays. (b) The mean square error as a function of T_m. The original image is a snapshot from a Gibbs distribution of the the $Q = 4$ ferromagnetic Ising model with 100×100 pixels and $T_s = 1.0$, $J_s = 1$ and $J = 1$. The halftone images are obtained by the uniform and uniform threshold $M = 1/2$.

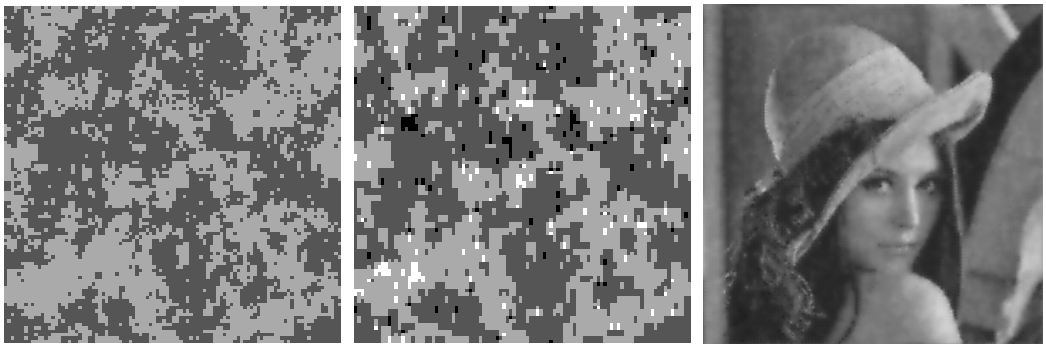

Figure 6: The left panel shows a $Q = 4$ grayscale image restored by the MPM estimate from the halftone image shown in Fig. 4 (left). The center panel shows a $Q = 4$ grayscale image restored by the MPM estimate from the halftone image shown in Fig. 4 (center). The right panel shows a $Q = 256$ grayscale image restored by the MPM estimate from the halftone image shown in Fig. 4 (right).

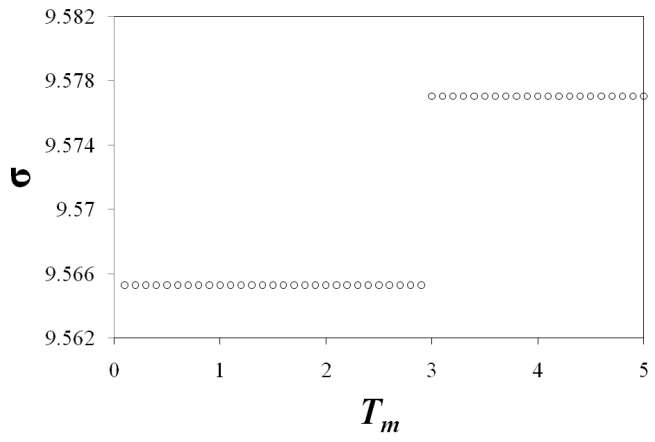

(a)

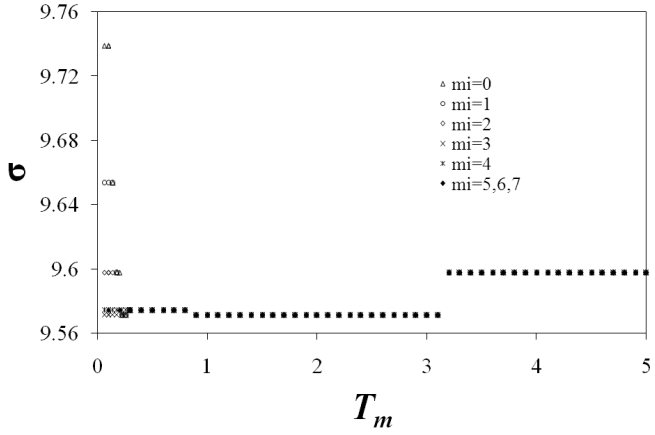

(b)

Figure 7: (a) The mean square error as a function of the parameter T_m when $Q = 8$, $T_s = 1$, $J_s = 1$, $M = (Q-1)/2$ and $J = 1$, (b) The mean square error as a function of the parameter T_m when $Q = 8$, $T_s = 1$, $J_s = 1$, $M = 4.5 \neq (Q-1)/2$ and $J = 1$. The value m_i for each line caption denotes the initial condition of the magnetization m to find the locally stable solution.

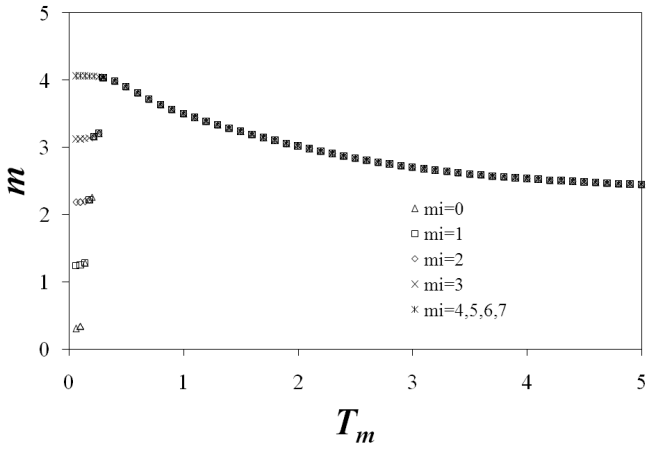

Figure 8: The magnetization m as a function of the parameter T_m when $Q = 8$, $T_s = 1$, $J_s = 1$, $M = 4.5 \neq (Q-1)/2$, $\tau = 0$ and $J = 1$.

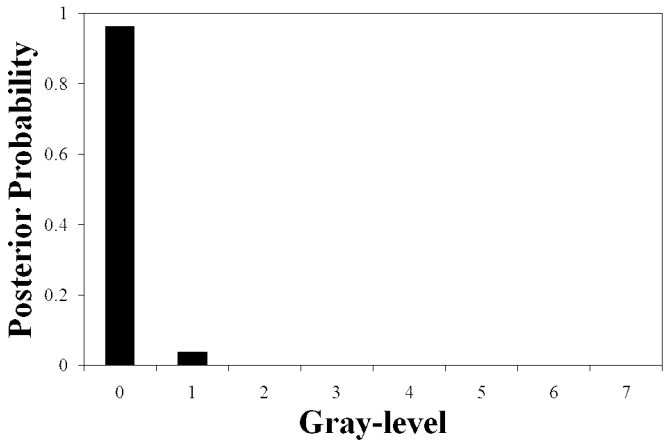

(a)

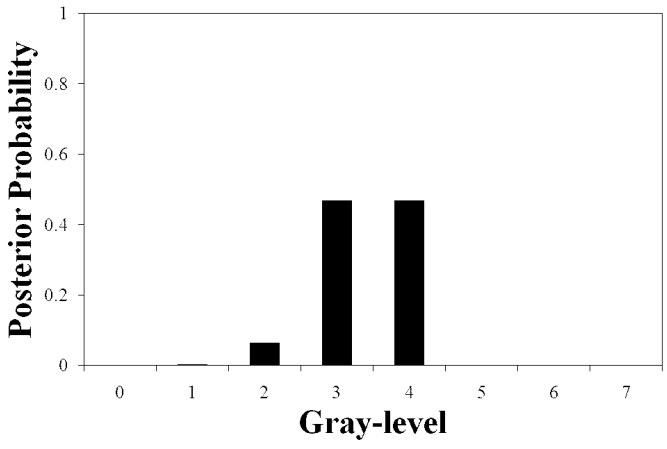

(b)

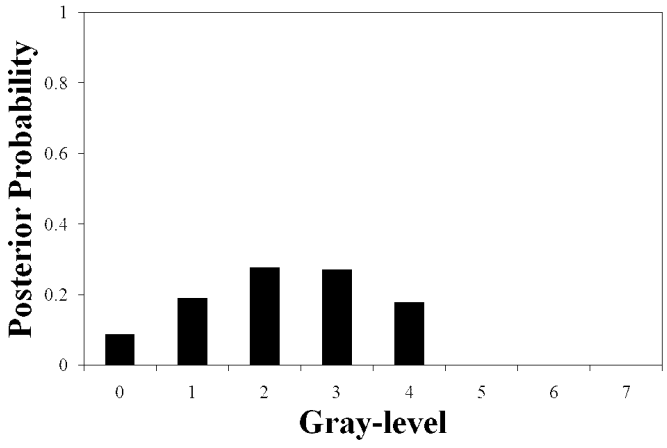

(c)

Figure 9: (a) The gray-level distribution of the restored image at $T_{\rm m} = 0.1$, (b) The gray-level distribution of the restored image at $T_{\rm m} = 1.0$, (c) The gray-level distribution of the restored image at $T_{\rm m} = 5.0$. Other paramegters are set as $Q = 8$, $T_s = 1$, $J_s = 1$, $M = 4.5 \neq (Q-1)/2$ and $J = 1$.

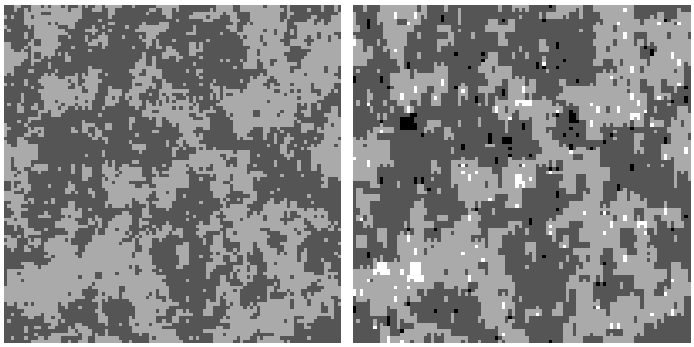

Figure 10: The left panel shows a $Q = 4$ grayscale image restored by the MPM estimate using the Bethe approximation from the halftone image shown in Fig. 4 (left). The right panel shows a $Q = 4$ grayscale image restored by the MPM estimate using the Bethe approximation from the halftone image shown in Fig. 4 (center).